

Spined hybrid soft robot for high speed, high force, tunable bistability, and wide-range stiffness modulation

Yichao Tang¹, Yinding Chi¹, Omid H. Maghsoudi², Jie Yin^{1*}

Affiliations

¹Applied Mechanics of Materials Laboratory, Department of Mechanical Engineering, Temple University, 1947 North 12th Street, Philadelphia, PA 19122, USA.

²Department of Bioengineering, Temple University, 1947 North 12th Street, Philadelphia, PA 19122, USA.

* Corresponding author. Email: jieyin@temple.edu

Abstract

The ease deformation of soft-bodied robots enables a variety of intriguing locomotion modes, yet their speed is typically slow owing to intrinsic soft materials limitation. Bioinspired by active actuation of spine deformation during high-speed galloping of cheetahs, the fastest animal on land, we propose spined hybrid soft bending actuators (SBAs) that enable high-speed locomotion and high force in soft robots. They are composed of rigid links as skeletal spines, SBAs as skeletal muscles, and an amplifier to enhance force output and velocity, as well as enable high precision, wide-range stiffness, and tunable snap-through instabilities. We demonstrated their integrations for a few high-performance soft machines, including high-speed yet energy-efficient crawlers with locomotion speed of 2.49 BL/s, fast-moving underwater swimmers (0.78 BL/s), soft grippers with over $\times 10^3$ stiffness modulation (maximum load capacity is 11.4 kg), bistable soft oscillators, and ultra-high-strength adhesive device that has ~ 700 N pull-off force.

INTRODUCTION

High-speed locomotion is an intriguing characteristic in quadrupedal mammals for prey capture or predator escape, as well as bioinspired running terrestrial robots for search-and-rescue and transportation (1). Among different locomotion gaits, galloping exhibits the highest running speed (2), e.g. the fastest galloping cheetah demonstrates a record speed of 29 m/s on land (3). Galloping has also been suggested as the most energy efficient mode of locomotion in quadrupedal mammals (4). The roles and benefits of spine flexion and extension for high-speed locomotion are well documented in terms of self-stabilization and elastic energy storage (5-7), largely benefiting the design of fast-speed and energetically economic legged rigid robots through spine actuation (8, 9).

Recently, soft robots have attracted tremendous research interest due to their potentially safe and adaptive interaction with humans and harsh environment, enabling a wide range of new functionalities that can hardly be achieved by conventional rigid robots (10), including manipulating delicate objects (11-16), navigating through a confined space (17, 18), and possessing multiple degrees of freedom (19-22). Despite the advances, it remains challenging to design high speed yet energy efficient locomotive soft robots due to the intrinsic limitations of their soft bodies. Normally, high speed locomotion requires fast response, large force output, high strain energy storage, and high precision motion of the actuators that are the merits of rigid robots. However, for soft-bodied robots, they often exhibit small force exertion and slow deformation response due to materials softness and structural compliance, thus it is hard to store high mechanical energy and precisely control soft body deformation, largely limiting their similar practical utilities as rigid robots in high-speed locomotion and high-strength object manipulation (23).

To address the challenges, a hybrid musculoskeletal system that combines soft materials as “muscles” and rigid links as “skeleton” may be a promising solution. Without sacrificing the benefits of rigid robots in high strength and accurate control, and soft robots in extreme compliance, the hybrid system makes it possible to simultaneously achieve compliancy and strength (24, 25). Inspired by the spine flexion and extension in high speed yet energy-efficient quadrupedal mammals such as galloping cheetahs (Fig. 1A), we propose here a bistable spined hybrid soft bending actuator, as schematically shown in Fig. 1B, that enables high force output, fast actuation speed, low energy consumption, tunable stiffness modulation, and high-accuracy deformation control. Very recently, bistability has been harnessed in soft robotics for untethered directional propulsion (26), autonomous control of air flow in soft bistable valves (27), and soft fluidic actuators with amplified responses (28). Different from the soft bistable elements in these examples, the hybrid soft actuator presented here is constructed from combining bistable rigid links as “skeletal spines” and soft pneumatic bending actuators as “skeletal muscles” (Fig. 1B). The rigid skeleton ensures precise deformation control and structural stability. It harnesses the rapid, switchable snap-through instability between two stable states actuated by the connected soft bending actuators. Unlike the limited energy storage in soft bistable structures due to low materials modulus, the mechanical energy is stored in a linear spring connecting the rigid spine, which can be tuned from low to high energy-storage capacity through simply pre-straining the spring. This spring in hybrid soft actuators acts as an active/passive amplifier. It not only enlarges the force and actuation speed through controllable snap-through instabilities, but also enables tunable stiffness and reduces energy consumption for the hybrid system. We demonstrate the ease of integrating the bistable spined hybrid soft bending actuator for high speed running soft crawlers on ground and fast-speed underwater fish-like soft swimmers with low energy consumption, as well as an adjustable high-strength gripper with wide-range variable stiffness modulation. We further extend the proposed hybrid strategy to soft dome-bending systems and demonstrate the use of spined hybrid soft doming actuator for bistable soft oscillator and high-strength adhesive pad.

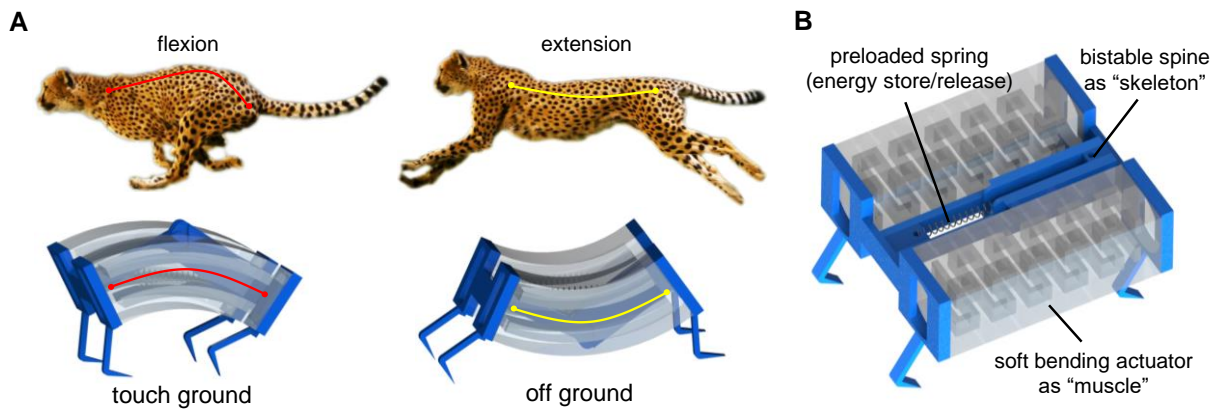


Fig. 1. Bistable spined hybrid soft bending actuators inspired by spine actuation during cheetahs' high-speed galloping. (A) - (B) Spine flexion and extension in cheetahs and the proposed bistable hybrid soft actuator (schematic shown in Fig. 1B) during energy efficient fast locomotion.

RESULTS

Bistable hybrid soft bending actuator

Fig. 2A shows the schematic design of the proposed bistable hybrid soft bending actuator (BHSBA). It consists of three components: two soft pneumatic bending actuators as skeletal muscles made of ecoflex, each with two layers of pneumatic channels (Fig. S1A), that can achieve switchable two-way bending upon pressurization to actuate flexion of the spine; a 3D printed flexible spine composed of two rigid hinged links as skeleton to provide structural rigidity for soft bending actuators (Fig. S1B); and a linear spring that connects two ends of the spine. To enable the snap-through bistability in the spine, the spring is pretensioned within the straight spine to store mechanical energy (middle of Fig. 2A). The straight spine represents an unstable state, and the bended configurations of the spine and its connected soft actuators, either to the left (right of Fig. 2A) or to the right, are the respective two stable states.

Fig. 2B shows the energy profile of the bistable bending actuator system as a function of the bending angle. The unstable state of State II at a bending angle of 0° , i.e. a straight configuration, possesses a local maximum energy U_{II} , and the two equilibrium and stable states possess the local minimum potential energy U_{eq} at the equilibrium bending angle θ_{eq} , also the maximum bending angle. θ_{eq} is determined by minimizing U_{eq} , which includes the strain energy in the bended soft actuator and the potential energy in the spring. Thus, the spring stiffness, spring pretension, and the material properties and geometry of the soft bending actuators all play a role in determining θ_{eq} , making it challenging for angle control. To precisely control the bending angle of the soft bending actuator in an ease yet programmable way, we set angular stoppers in the spine to block its rotational movement at the preset lock angles of θ_1 and θ_2 (top right of Fig. 2A), the value of which is smaller than θ_{eq} . Correspondingly, we choose a relatively large-stiffness spring with pretension to readily satisfy the requirement of both $U_{II} > U_I$ (or $U_{III} > U_{eq}$ and θ_1 (or θ_2) $< \theta_{eq}$ to enable bistability and precise deformation control, where U_I and U_{III} denote the potential energy of the locked states (Fig. 2B), so that the lock states will represent the resting stable states.

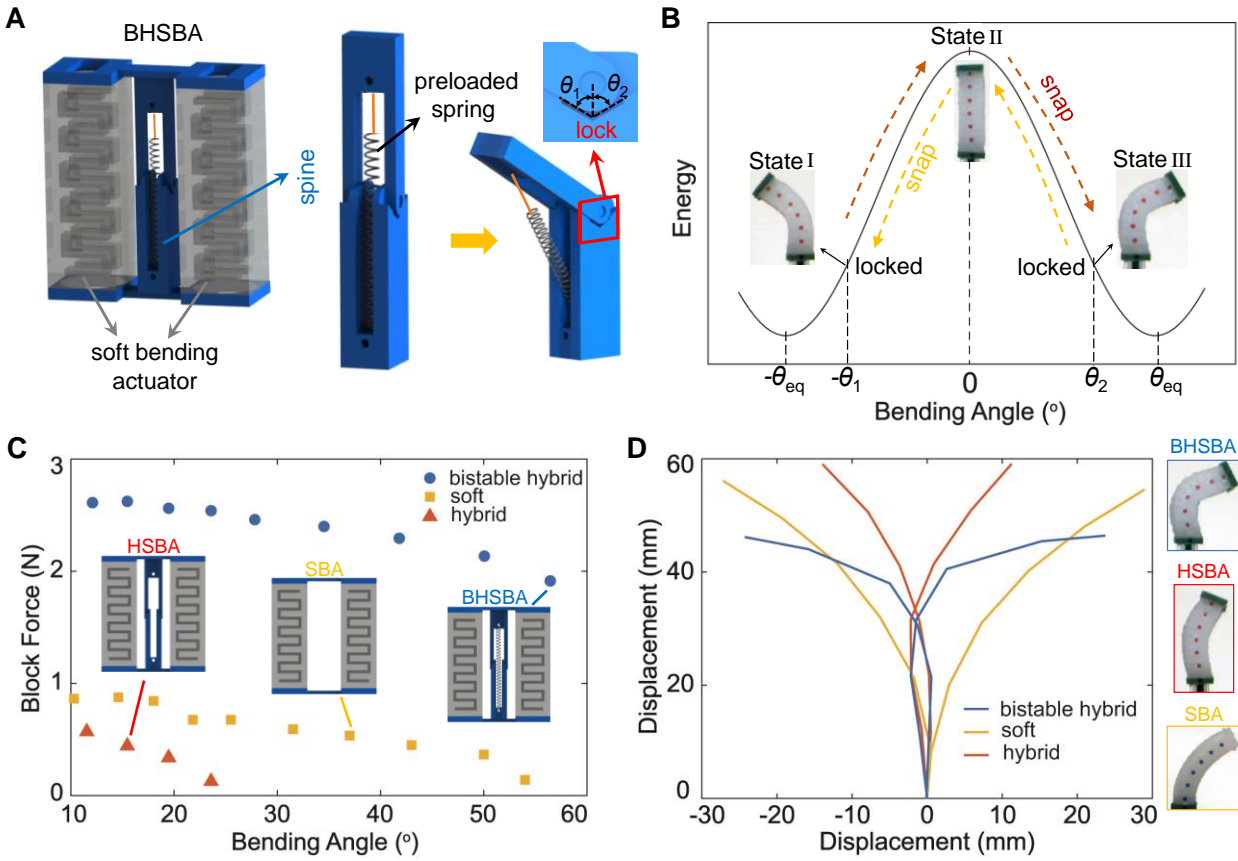


Fig. 2. Bistable hybrid soft bending actuators (BHSBA). (A) Schematic of the three components based BHSBA: two 2-way pneumatic soft bending actuators (left); a rigid rotational spine that provides precision (through locking structures) and overall strength (middle); a pretensioned spring that enables snap-through instabilities (right). (B) Schematic potential energy of BHSBA vs. bending angle. The rest states (I and III) are the angular locked states and State II is the unstable state. Local minimum energy states are the equilibrium states. Insets are the actuated shapes of the prototype at each state. The energy barrier is mainly determined by the spring properties (stiffness and pretension). (C) Block force vs. bending angle of BHSBA and its two counterparts: hybrid soft bending actuator (HSBA) without spring and soft bending actuator (SBA) without both spines and springs. All actuators are pressurized at 30 kPa. Insets are schematics of front views of the three actuators. (D) Motion tracking of BHSBA, HSBA, and SBA at their maximum bending angle under the same actuation pressure of 30 kPa with their actuated shapes shown on the right.

The working mechanism of BHSBA is straightforward: at a rest state of bended shape, e.g. State I in Fig. 2B (left inset), after inflating the exterior layered pneumatic channel of the bending actuators, it will bend toward the unstable planar state, i.e. State II (middle inset), where the spring stores the most energy, and then rapidly snap to another stable state, i.e. State III (right inset). This process can be easily reversed from State III to State I by actuating the other side of channeled layer in the bending actuators. Thus, the actuator can generate a swing motion between two stable states. The energy barrier (E) of this bistable system can be obtained as (Supplementary Materials):

$$E = U_{II} - U_I = U_{\text{spring, II}} - (U_{\text{spring, I}} + U_{\text{actuator, I}}) \quad (1)$$

where $U_{\text{spring, I}}$ and $U_{\text{spring, II}}$ are the potential energy of the spring at State I and State II, respectively. $U_{\text{actuator, I}}$ is the potential energy of the bending actuator at State I. Here we assume free rotation of

the center joint in the rigid spine and the same lock angle ($\theta_1 = \theta_2$) for State I and State III. By introducing the spring properties (assume linear stiffness) into Eqn. (1), we can get:

$$E = \frac{1}{2} k_{\Delta} x^2 \cdot \sin^2(\theta_1/2) - U_{\text{actuator,I}} \quad (2)$$

where k is the spring stiffness and Δx is the pre-extension of the spring at State II.

To examine the power-amplifying-effect enabled by bistability, we compare the actuation performances of BHSBA with its two bistability-disabled counterparts, including the block force, motion, and speed. One is the hybrid soft bending actuator (HSBA) after removing the spring in the BHSBA (left inset of Fig. 2C), corresponding to the extreme case of $k = 0$ to disable the bistability, and the other is the soft bending actuator (SBA) without both spines and springs (middle inset of Fig. 2C). The three actuators with their bottom fixed are pneumatically actuated at the same pressure of 30 kPa and the same frequency of 3.2 HZ during the swing motion (Fig. S2 and Table S1). The spring stiffness k is 0.53 N/mm and the pretension in the spring is 5mm. The lock angle in the spine is $\theta_1 = \theta_2 = 60^\circ$.

Fig. 2D shows the tracking trajectories of deformed shapes at rest states with maximum bending angle θ_{\max} during swing motion of the three actuators. Compared to its soft ($\theta_{\max} \sim 55^\circ$, bottom right of Fig. 2D) and hybrid ($\theta_{\max} \sim 25^\circ$, middle right of Fig. 2D) counterparts, the BHSBA exhibits the largest θ_{\max} (top right of Fig. 2D), which is equal to the lock angle since it cannot bend beyond 60° (Movie S1), demonstrating a more precise control in the bending motion. We note that the soft bending actuator (i.e. SBA) shows the largest deflection, resulting from both axial elongation and bending deformation, whereas the axial elongation in the BHSBA is largely constrained by the rigid spine for a dominated bending deformation. Thus, it is ease to predict the bending angle and curvature of the BHSBA in a controlled fashion despite the difficulty in predicting the SBA due to the axial elongation (see Supplementary Materials for more details). Fig. 2C shows the corresponding measured block force F_b as a function of bending angle. As expected, the SBA generates a small block force of less than 1N due to its materials compliance, which is slightly higher than the hybrid soft bending actuator (i.e. HSBA). In sharp contrast, F_b is significantly enhanced to the range of 2-2.8N in the bistable hybrid actuator, which is approximately 3 times larger than the SBA and 7 times larger than the HSBA when compared at the same bending angle of 20° , demonstrating the benefit of bistability in amplifying the output force capability.

In addition to precise bending angle control and output force amplification, the proposed bistable hybrid system (i.e. BHSBA) also contributes to an increasing velocity and energy saving for motion. For a target swing motion with a swing angle of 60° , the BHSBA takes the shortest half-period $t_{\text{hp}} = 0.13$ s swinging from -60° to 60° under the lowest pneumatic pressure of 30kPa. In contrast, its counterpart SBA requires ~ 38 kPa pressure with $t_{\text{hp}} = 0.16$ s and HSBA requires ~ 80 kPa pressure with $t_{\text{hp}} = 0.27$ s (Movie S2). Therefore, the BHSBA consumes less energy to achieve the same bending angle, while still producing a significantly higher reaction force ($F_b = 1.92$ N) compared to its two counterparts ($F_b = 0.12$ N for SBA and 0.16 N for HSBA at 57°), which are attributed to the release of stored energy in springs through snap-through bistability.

Despite recent advances in harnessing bistable soft structures for design of soft robotic systems (26-28), our bistable hybrid actuator provides a few potential advantages compared with these emerging compliant bistable structures: (1) Bistable entirely soft structures can only store limited amount of energy due to low modulus. However, the proposed bistable hybrid system possesses a larger energy-sortation capacity owing to the integrated high-stiffness spring, thus exhibiting better performance in amplifying force and velocity. (2) The two rest states of bistable soft structures are always energetically inequivalent, i.e., the as-fabricated state is always more stable than the other stable state. However, the two stable states of the proposed bistable hybrid actuator can be

manipulated to be energetically equivalent or biased by simply tuning the two independent lock angles θ_1 and θ_2 with $\theta_1 = \theta_2$ or $\theta_1 \neq \theta_2$. This flexibility in adjusting the biased rest states could be beneficial for building multistable and directional systems (26). (3) Unlike the fixed energy barrier in most of the bistable soft actuators, one can easily tune the energy barrier of the proposed bistable hybrid bending actuator by changing either the pretension in the spring or the spring stiffness in terms of Eq. (2), thus resulting in tunable force exertion and response speed for potential targeted and programmable performances.

High-speed bistable spined crawler

Bioinspired by the similar flexion and extension motion of the flexible spine during the high-speed galloping in mammals such as the fastest land animal cheetah (Fig. 3A), we explore harnessing the bistable spine enabled power amplification and fast response for its potential application in high-speed yet energy efficient locomotive soft robots. As schematically illustrated in Fig. 1B, simply attaching four claws to the BHSBA (i.e. spined soft body) constitutes the proposed high-speed hybrid soft robot with a bistable spine. The prototype is 7 cm long and 6 cm wide with a weight of 45g. The spring stiffness k is 0.53 N/mm and the pre-extension is 5mm. The lock angle of the spine is $\theta_1 = \theta_2 = 60^\circ$. Small ecoflex pads are attached on the claws, as shown in Fig. 2B, to break the deformation symmetry through providing passive switchable friction for front and rear claws (29). At the rest state, its soft body is initially bent downward (top of Fig. 3B), the front legs have much larger static friction force (because ecoflex contacts the surface) than the rear ones (right of Fig. 3B). This will generate a forward motion when the soft body is actuated and bending upward; when the crawler is taking a convex shape, i.e. bend-up (bottom of Fig. 3B), the rear legs will have larger friction force than the front ones. This also results in a forward locomotion when the body is actuated and bending downward.

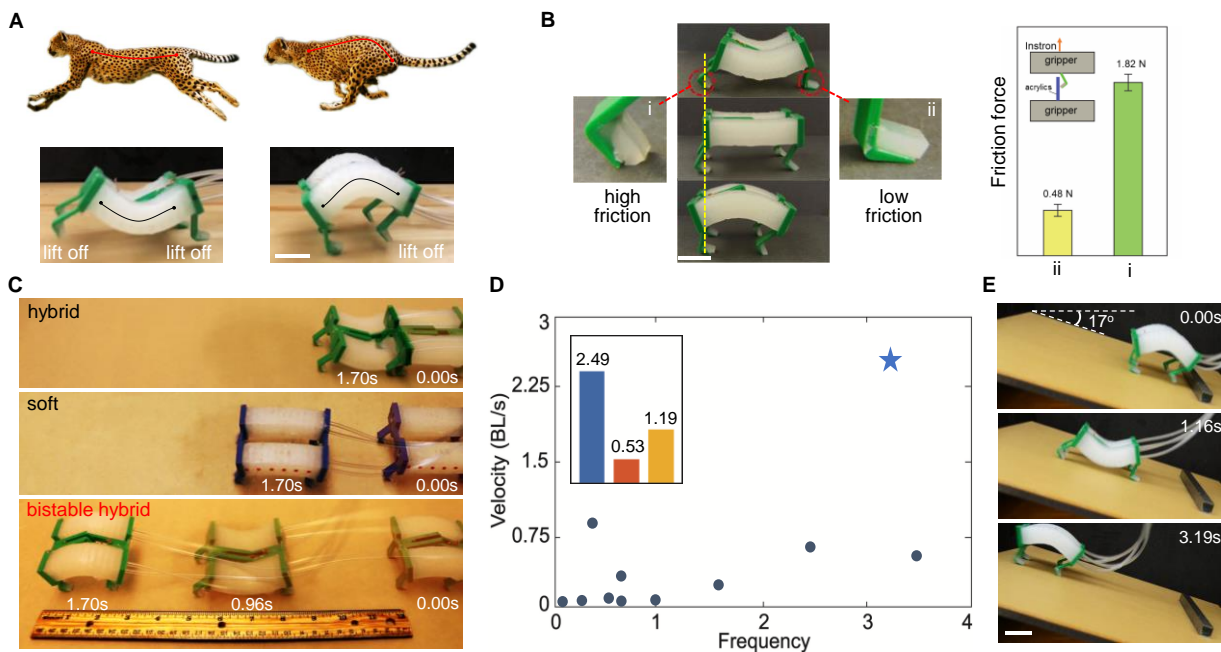


Fig. 3. High-speed spined crawler based on BHSBA. (A) Locomotion gaits of the proposed spined crawler inspired by the spine actuation in the fastest galloping cheetahs. The spine bends upward to store energy when touching ground and bends downward to release energy and extend its stride length with legs lifting off the ground during the high-speed locomotion. (B) Left: Mechanism of directional locomotion. The ecoflex pads attached to the claws provide friction force and transit the symmetric bending of BHSBA into a directional locomotion. Right: static friction forces of claws with and without ecoflex pad-substrate contact. The claw shows ~280% increase in the friction force (1.82 N) when the attached ecoflex pad contacts the substrate. Inset shows the schematic of

friction force measurement. (C) Demonstration of locomotion in the high-speed spined crawler and its two counterparts at different actuation time: soft crawler based on SBA and hybrid soft crawler based on HSBA. The bistable hybrid soft crawler shows the fastest speed. (D) Comparison of locomotion velocity measured in body length per second (BL/s) between our proposed bistable hybrid soft crawler (denoted as star-shaped symbol) and reported locomotive soft robots in literatures. The inset is the locomotion speed of the high-speed spined crawler and its two counterparts. (E) Demonstration of the proposed bistable hybrid soft crawler's capability in climbing slightly titled surfaces (tilting angle of 17°). The other two counterparts fail to climb. The scale bar is 25 mm.

Despite the simplicity of the design, the proposed bistable hybrid soft crawler exhibits a superior high locomotion speed. It can achieve a linear locomotion speed of 174.4 mm/s, or 2.49 BL/s when pressurized at 30 kPa (average actuation frequency is 3.2 Hz, Fig. S2 and Table S1) on a wood top (bottom of Fig. 3C and inset of Fig. 3D). Such a high locomotion speed is 2.1 times the speed of its counterpart soft crawler based on SBA (middle of Fig. 3C and inset of Fig. 3D), and 4.7 times the speed of the hybrid soft crawler based on HSBA with spring removed (top of Fig. 3C and inset of Fig. 3D). The comparison of real time locomotion video can be found in Movie S3. The slow motion of the bistable hybrid soft crawler (Movie S4) shows that its locomotion gait is similar to that of high-speed cheetahs during their energy-economic galloping (Fig. 3A). The forefeet are set down to bend up its back to store energy before they lift off (right column of Fig. 3A), and then straightening and bending downward to lengthen the stride by extending the forefeet with all feet off the ground (left column of Fig. 3A). In contrast, for the other two counterparts, all the feet always remain contacted with the ground and thus consume more energy to overcome the friction (Movie S3). Note that different from the power supply from muscles and tendons in legs and back of the animal, the energy storage and quick release in the bistable hybrid soft crawler are triggered from the snap-through bistability in the spine, which will help to save energy cost and enable large force exertion and fast response for high-speed locomotion. We further test its locomotion capability on a tilted surface. We find that when the walking surface is tilted to 17° , the bistable hybrid soft crawler can still achieve a fast location speed of 0.56 BL/s (Fig. 3E). However, the other two counterparts are not capable of climbing such tilted surfaces (Movie S5).

In Fig. 3D, we compare the locomotion velocity of the proposed bistable hybrid soft crawler with a few previously reported locomotive soft robotics (20, 29-38). These soft robots, mostly possessing continuous compliant bodies, demonstrate a relatively slow speed in the range of 0.02 – 0.5 BL/s due to either slow actuation speed or small force exertion of the composed soft actuator. In sharp contrast, the proposed bistable hybrid soft crawler is much faster, meanwhile costing less energy input (it only requires 30 kPa pressurization to perform) due to the benefit of rigid skeleton and force amplifier, which is even comparable, in velocity, with some rigid robots and terrestrial animal (1 – 100 BL/s). It should be noted that, the stored energy in spring, which can be tuned by changing spring stiffness or pretension, plays a dominant role in its energy barrier, thus affects its force output, velocity, and energy efficiency. Ideally, using a large energy-stored spring will generate a large energy gap, thus corresponding to a large force exertion from the bistable hybrid system. However, meanwhile, the high energy spring will increase the energy consumption of the bistable hybrid system because it requires more energy input to overcome the high energy barriers. It may lead to a drop in the frequency and velocity of the bistable hybrid system unless increasing the input signal strength (e.g. air flow rate). Therefore, a trade-off should be considered for selecting the stiffness and pretension of the spring for design of high-speed locomotive robots, the details of which will be studied in the future to optimize the performance of the proposed high-speed crawler.

Fast speed underwater swimmer

In addition to a potential terrestrial high-speed locomotive soft robot, the similar swing motion of their soft body in fishes inspires us for exploring its multifunctionality as a potential fast speed underwater robot. The structure of this fish-mimicking swimming robot is depicted in Fig. 4A. It is composed of an encapsulated BHSBA (e-BHSBA) and an attached thin plastic sheet-based fin (thickness = 0.25mm) at its rear for enhancing the propulsion force. For underwater locomotion, compared to on-land locomotion, it requires a relatively larger output force to overcome the water resistance for propulsion due to the fluid-solid interaction. Therefore, for pneumatic bending actuator-based swimmer, it needs more energy input through a high actuation pressure of over 150 kPa, which could lead to the structural failure of its soft body if not strengthened. To enhance the force output and structural reliability, we encapsulate the soft bending actuators with conformable, stretchable, and bendable polymeric wrinkling-based envelope by following Cianchetti et al. (39), as highlighted in red color of wrinkled skin in Fig. 4A. When protected with braided sheath, the bending actuator can sustain higher pressure and survive longer fatigue-life (39), therefore here we use the encapsulated soft bending actuator for under water locomotion. The bending actuator is 45 mm in length and 25 mm in diameter. The whole prototype is ~150 mm long with a mass of 51g. The lock angle of the spine is 45°. The spring stiffness is 1.09 N/mm with 10 mm pre-extension.

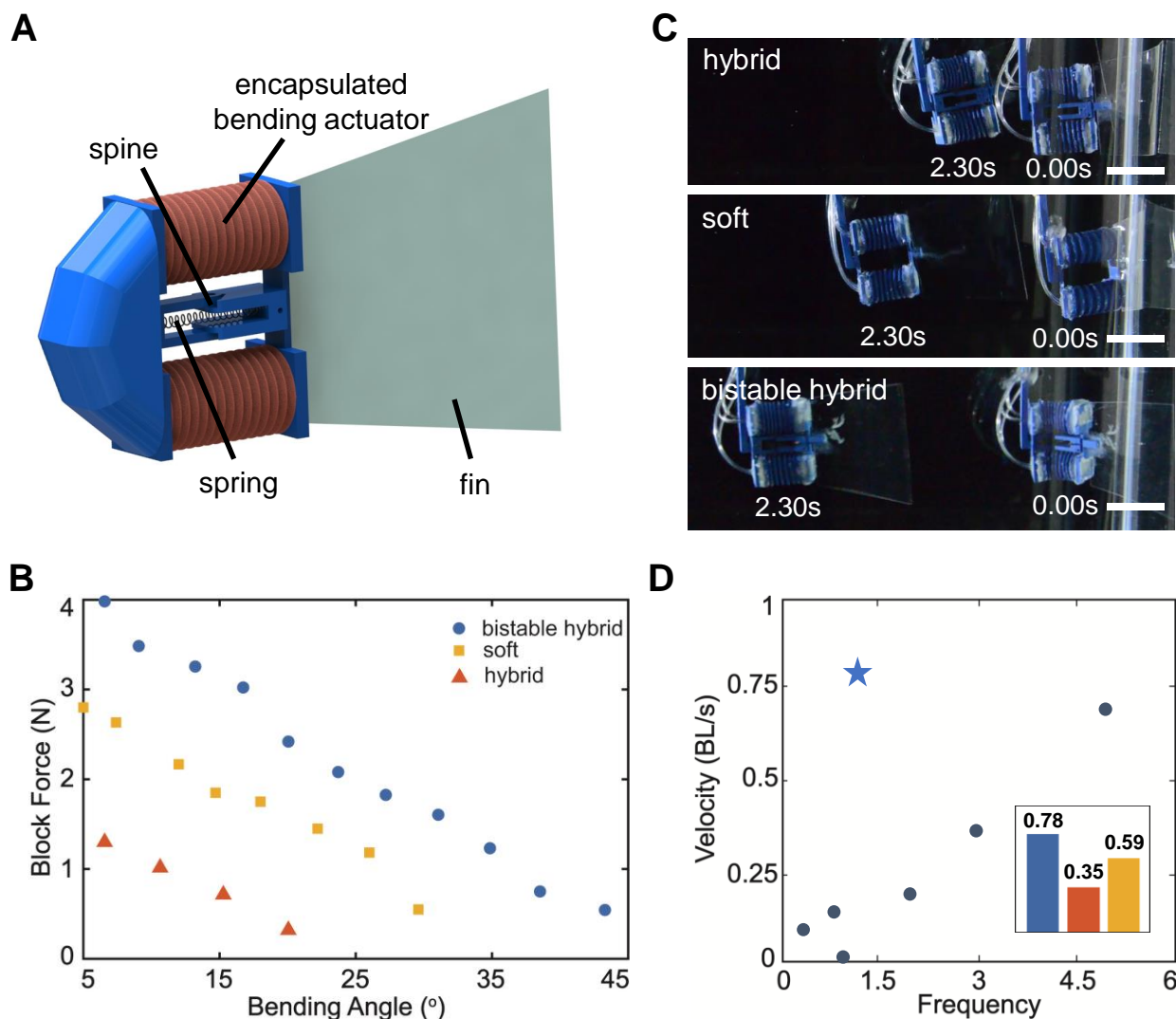


Fig. 4. Fast-speed underwater fish-like soft robot based on encapsulated BHSBA (e-BHSBA). (A) Schematic of the proposed fish-like robot, which is composed of an e-BHSBA attached with a polymeric fin. The schematic head is for decoration purpose only. (B) Comparison in block force vs. bending angle of e-BHSBA, e-HSBA, and e-SBA. All actuators are pressurized at 160 kPa. (C)

Demonstration of underwater locomotion in bistable hybrid soft swimmer and its two counterparts at different actuation time: soft swimmer based on encapsulated SBA and hybrid soft swimmer based on encapsulated HSBA. The bistable hybrid soft swimmer shows the fastest speed. The scale bar is 50 mm. (D) Comparison of swimming velocity between the proposed bistable hybrid soft fish-like robot (denoted as star-shaped symbol) and various reported underwater soft swimmers (denoted as round symbols). The inset is the swimming speed of the bistable hybrid soft swimmer and its two hybrid and soft counterparts.

We measure the block force and deformation of the e-BHSBA and compare with its two bistability-disabled counterparts encapsulated HSBA and SBA under the same pneumatic pressure of 160kPa. As expected, the BHSBA generates the largest maximum block force over 4 N and maximum bending angle θ_{\max} of 45° , which is equal to the preset lock angle in the spine. In contrast, its two hybrid and soft counterparts show smaller force exertion and bending angle (Fig. 4B).

Fig. 4C shows the comparison of swimming speed between the proposed bistable hybrid soft swimming robot and its two counterparts under the same pneumatic pressure of 160kPa and average frequency of 1.3 Hz (Fig. S2 and Table S1): soft swimmer based on encapsulated SBA and hybrid swimmer based on encapsulated HSBA. It shows that the bistable hybrid soft swimming robot can achieve a maximum average locomotion speed of ~ 117 mm/s (bottom of Fig. 4C), or 0.78 BL/s, which is 32% and 122% faster than its two counterparts: soft swimmer (middle of Fig. 4C) and hybrid swimmer (top of Fig. 4C), respectively. The comparison of real time underwater locomotion between the three swimmers can be found in Movie S6.

We further compare the swimming performance of our proposed bistable hybrid soft swimmer with other reported soft swimming prototypes, which are under different actuation methods and frequencies (Fig. 4D) (40-45). It shows that despite different actuation methods, the swimming velocity is found to approximately follow a monotonically increasing trend with the actuation frequency, arriving at a high speed of 0.7 BL/s at 5 Hz in the system of a manta ray-inspired electronic fish (42). In contrast, despite a relative low average actuation frequency of 1.3 Hz, the proposed bistable hybrid soft swimmer can achieve a slightly faster speed of 0.78 BL/s (star-shaped symbol), largely outperforming most of the reported soft swimmers (round symbols). Although it is still slower than biological fishes which exhibit a swimming capability of 2-10 BL/s (46), future work on further optimization of the bistable structure, actuators, springs and the morphology of the robot may be able to fill this gap.

Bending actuators with tunable stiffness

With the flexibility in manipulating the tension in the spring, next, we further explore the stiffness modulation of the hybrid soft bending actuator for potential applications in strength-adjustable soft grippers. Stiffening/softening is an important issue for soft robotics in maintaining their shape changes and realizing adaptable force exertion to different working environment. Extensive research efforts have been dedicated to building soft robotics with variable stiffness by harnessing granular jamming (16, 20, 47), phase change (48, 49), glass transition (50, 51), and tendon-driven-stiffening (13, 52). We employ the similar tendon-driven stiffening strategy to stiffening our hybrid soft-rigid system. Despite the ease in implementation, we demonstrate its effectiveness in manipulating the stiffness in a controlled fashion as below.

Fig. 5A shows the schematic of our proposed design, which is similar to the e-BHSBA in Fig. 4A. The difference is that we connect a DC motor-driven tendon to the end of the extension spring. When the DC motor is triggered, it will pull the tendon and thus extend the spring, resulting in bending of the actuator towards the lock state. Further extension of the spring beyond the lock state can significantly stiffen the e-BHSBA. For this tendon-spring-driven system, the spring stiffness

plays a dominant role in determining the stiffening modulation, thus, using a high-stiffness spring will ensure a large amplification in stiffness. To verify this effect, we characterize the bending stiffness of e-BHSBA as a function of the spring extension (Fig. S3). Two different base-constraining conditions are compared, which are shown in the insets of Fig. 5B and Fig. 5C, respectively. In both tests, BHSBA is bent at 80° (the lock angle in the spine is $\theta_1 = \theta_2 = 85^\circ$) with its free end blocked by a force sensor. Simultaneously, the motor is pulling the spring (the spring stiffness is 9.67 N/mm) and the bending actuators are pressurized at 120kPa. The experiment results (Fig. 5B) shows that its block force can be manipulated between 0.1 – 103 N by tuning the length of the spring, which agrees well with the simple theoretical model (see Supplementary Materials for details). It indicates an over $\times 10^3$ variation in stiffness modulation by harnessing the spring-tendon-stiffening system, which is difficult to be achieved by most previously reported stiffening methods used for pneumatic actuators (47, 48, 51). In addition, unlike a few stiffening mechanisms only allowing for dual (or limited) stiffness control (53, 54), the proposed stiffening strategy demonstrates a continuous tunability in stiffness by continuously tensioning the spring, thus providing the potential in constructing multiple-stiffness soft engineered systems.

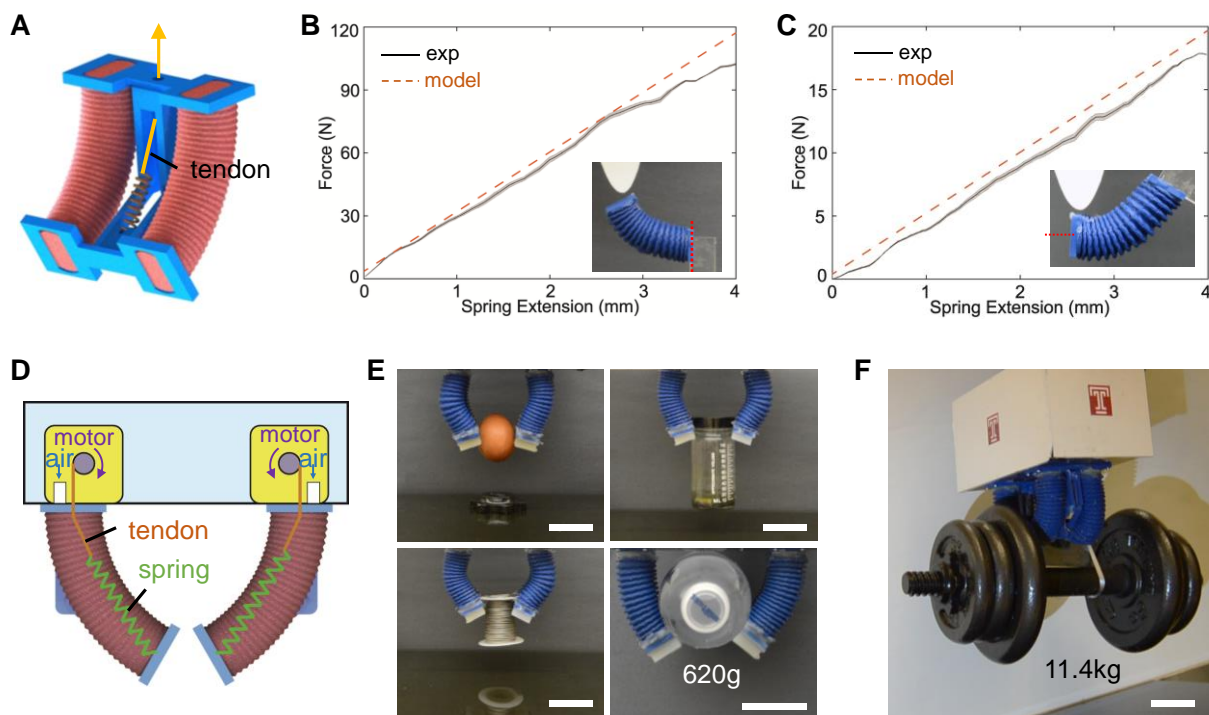


Fig. 5. Hybrid soft grippers with wide-range variable stiffness modulation based on e-BHSBA. (A) Schematic of e-BHSBA driven by tendon. (B)-(C) Stiffness test of e-BHSBA (bent at 75°) under two loading conditions (insets). We characterize the force as a function of spring extension. The solid line is the mean of three experiments (with shaded error bar) and the dashed line presents the theoretical model result. (D) Schematic illustration of the proposed gripper by assembling two e-BHSBAs. The manipulation can be controlled by both motors, through pulling the spring, and pneumatic signals. (E) Demonstrations of its capability in grasping various objects in different shapes and weight. (F) Demonstration of high-load manipulation. The scale bar is 50 mm.

Taking the advantage of this wide-range modulation and programmable stiffness, we design and fabricate a strength-adjustable hybrid soft gripper, which allows for manipulating a variety of target objects ranging from fragile lightweight to high-load objects. As schematically shown in Fig. 5D, the gripper is composed of two e-BHSBAs, each one can be driven by both pneumatic signals and DC motors. Pneumatic actuation is used for gripping lightweight and fragile objects by utilizing

the intrinsic compliance of soft materials/structures. This soft gripping requires the tendon to be relaxed and thus the spring remains inactive, while motor-driven actuation is used for grasping heavy objects through pulling the spring to amplify the bending stiffness. Based on this simple working mechanism, we successfully demonstrate that the proposed hybrid soft gripper can easily pull off objects in a variety of shapes, sizes, and weights. For example, when pressured at 90kPa without activating the tendon, i.e. the tendon and spring remain relaxed, the gripper is capable of grasping fragile fresh egg, small-sized reagent bottle, steel wraps, and tape roll in regular spheroidal or cylindrical shapes as shown in Fig. 5E and Movie S7. When driven by motors, the gripper is capable of directly grasping much heavier objects such as a bottle of water (620g, bottom right of Fig. 5E) and a maximum of 3.6 kg payload of dumbbells by wrapping around the objects (Movie S7). The grasping payload can be further enhanced by pulling through the gripper’s “finger” tips, for example, a 9.2 kg payload of dumbbells (Movie S7). Currently, the largest payload that our gripper can grasp is 11.4 kg (25.3lb), as demonstrated in Fig. 5F and Movie S7, which is ~180 times the weight of a single e-BHSBA. For all the tests, we use the same high-stiffness spring ($k = 9.67$ N/mm) and it is stretched by 3 mm at the lock state for grasping the maximum payload. It should be noted that the gripping force of our gripper is mainly determined by the spring force, therefore, its gripping capacity can be further improved by using stronger springs. More details and gripping videos can be found in the Supplementary Materials.

Hybrid soft doming actuator as soft oscillator

By replacing the soft bilayer tubular-like structures with soft bilayer disk-like plates, we further extend the bistable hybrid strategy to dome-bending based actuators for improved performances (30, 55). Fig. 6A shows the schematics of the proposed bistable hybrid soft doming actuator (BHSDA). It is composed of a two-way doming actuator with the rigid spine laminated between two spiral-channeled layers to bend upward or downward. Different from the pretensioned spring in the tubular-based bistable bending actuator, we rather use pre-compressed springs to enable the bistability (Fig. 6B). We use four sliding beams together with respective compression springs as the bistable spine-like skeleton (Fig. S4). Fig. 6C schematically illustrates the working mechanism. Since the springs are pre-compressed, the BHSDA at rest states will possess a dome-shape. By actuating either layer of the bilayer spiral channels, BHSDA at equilibrium state (State I) deforms back to the unstable planar disk state (State II), and then rapidly snap through to another equilibrium state (State III). This process can be reversed from State III to State I by actuating the other channeled layer. The energy barrier of this bistable system is determined by Eqn. (1), where U_{actuator} , here is the potential energy of the doming actuator at rest states. Since there is no lock structure, the minimal-energy states of BHSDA present its rest states.

To verify the role of bistability in amplifying force, we characterize the reaction force of BHSDA and compare it with the block force of hybrid soft doming actuator (HSDA) without spring and soft doming actuator (SDA) without both spined skeleton and springs. BHSDA has 68 mm in diameter and 24 mm in thickness. The stiffness of the compression spring is 1.21 N/mm and is compressed by ~ 6.3 mm at planar state (State II, top left inset of Fig. 6C). The block force is measured by positioning the actuator under a force gauge leaving a distance d between them (inset of Fig. 6D) and applied pressure of 80 kPa. The result (Fig. 6D) shows that BHSDA exhibits a much larger reaction force than that of its two soft and hybrid counterparts. At $d = 4$ mm, BHSDA demonstrates a 31.2 N block force, while HSDA and SDA only generate 9.6 N and 2.8 N, respectively, indicating ~3.2 times and ~11.1 times force amplification. Based on this amplified force output and the snap-through instability, the proposed BHSDA shows the potential as a large-force bistable doming oscillator (Movie S8). The oscillation is achieved through periodically actuating the two pneumatic channels in sequence with constant pressure of 100 kPa and frequency of 0.91 Hz (Fig. S2 and Table S1). This oscillatory behavior in BHSDA could find potential

applications in design of soft valves (27), underwater locomotive robots (44), jumping robots (56, 57), and grippers.

Hybrid soft doming adhesion actuator

Compared to the tubular-based soft bending actuator, the uniqueness of soft pneumatic doming actuators lies in enabling adhesion when attached to a surface driven by doming deformation (30, 55). However, the adhesion strength of entirely soft doming actuators is largely limited by the intrinsic materials softness and the bifurcated bent structure (Fig. S5) under high pneumatic pressurized actuation (55, 58). To overcome the limitation, we use the same hybrid strategy by integrating the stiff spined skeleton with the soft doming actuator muscles.

Fig. 6E shows the schematic design of the proposed hybrid soft doming adhesion actuator (HSDAA). Different from the bistable hybrid soft oscillator actuated by two-way doming and release of stored energy in springs, the hybrid soft adhesion actuator has only one layer of spiral pneumatic channel on the top to actuate the dome-up deformation for enabling adhesion, and the rigid spine is underneath the pneumatic channel. The prototype is 120 mm in diameter and 12 mm thick with a mass of 175 g (Fig. S6).

The working mechanism of doming based adhesion is simple: when the top lay pneumatic channel is pressurized, as shown in the inset of Fig. 6F, it will deform into a dome shape, generating a nearly vacuum cavity between the structure and the target surface (30, 55). The pressure difference between the cavity and the atmosphere will force the actuator to firmly attach to the substrate. The adhesion strength is mainly determined by the pressure difference and the structural stability (55). Thus, no springs are applied to the rigid spine to eliminate bistability. The 6-beam rigid skeleton (Fig. S7) shows single degree-of-freedom in motion (either pop-up or pop-down), thus only allows the actuator to undergo an axisymmetric deformation regardless of input pressure, therefore it can effectively prevent the actuator from deforming into an asymmetric and bifurcated configuration.

To reveal the role of the skeleton in affecting this doming based adhesion, we examine the adhesion strength of HSDAA by measuring its pull-off force on an acrylics surface. Fig. 6F shows that the HSDAA (pressured at 80 kPa) can bear considerable pull-off force, measuring over 700 N, which is ~400 times the weight of the prototype. In sharp contrast, its counterpart entirely soft doming actuator with the same geometry exhibits a much lower normal adhesion strength of ~112N. Utilizing this over 6-folds improvement in adhesion, we demonstrate that HSDAA is capable of holding the weight of a female adult (52 kg), as shown in Fig. 6G and Movie S9 (see Fig. S6 for the experimental setup). This high-load capacity of HSDAA allows future research in building high-strength soft adhesive devices for potential applications in object transportation (16), climbing robot (30, 59), and underwater gripping (60) by harnessing the spine-guided doming.

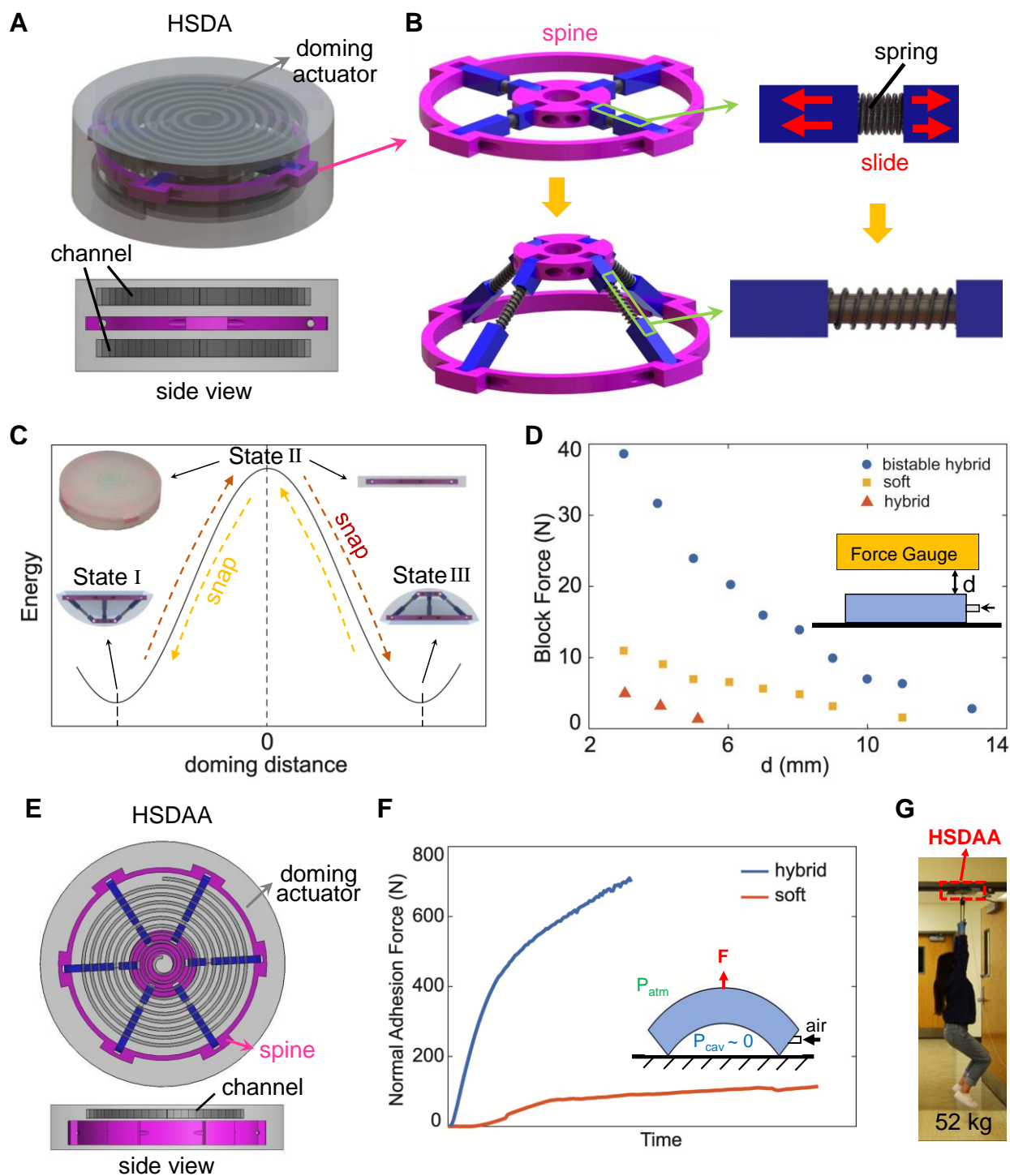


Fig. 6. Hybrid soft doming actuators. (A) Schematic of bistable hybrid soft doming actuator (BHSDA). (B) Schematic of the integrated rigid skeleton in BHSDA. Compression springs are incorporated into the spine to enable snap-through instability. (C) Schematic potential energy of BHSDA vs. doming distance. Insets show the schematics of actuated shapes at three stable/equilibrium (State I and III) and unstable states (State II). Top-left inset shows the prototype at unstable State II. (D) Block force of BHSDA, hybrid soft doming actuator (HSBA) without springs and entirely soft doming actuator (SBA) measured under 100 kPa. (E) Schematic of hybrid soft doming adhesive actuator (HSDAA). It is composed of a pneumatic soft doming actuator enclosed with a multi-beam rigid spine underneath the pneumatic spiral channel. (F) Pull-off force of HSDAA and its counterpart entirely soft doming adhesive actuator (SDAA) on acrylics surfaces

(pressurized at 80 kPa). The inset shows the adhesion mechanism. (D) Demonstration of HSDAA holding an adult female with weight of 52 kg.

DISCUSSION

We demonstrate that by integrating with rigid skeleton and amplifier, the mechanical performances of soft bending actuators and soft doming actuator can be largely improved, including enlarged force, amplified speed, lower energy consumption, tunable bistability, and programmable stiffness. This paper serves as a design guideline for building such hybrid soft actuators/robots. Although we only demonstrate the integration of our hybrid actuator in building high-speed locomotive robots and high-strength manipulators, the high force output without sacrificing the benefit of soft robots could find potential applications in surgical robot (21, 61), medical robot (62), and wearable device (15, 63). The proposed bistable hybrid system opens a new avenue for constructing large-force and high-speed soft robotics, and we envision that it could inspire more further exploration in building larger-scale ($\geq 10^1$ cm) soft robots.

Despite the use of conventional pneumatic soft actuators in our demonstrated hybrid system, the proposed technique could be potentially expanded to other types of soft actuators (such as fiber-reinforced and dielectric actuators) in response to other actuation signals including heat, electricity, and light. We believe that the proposed hybrid system could significantly improve their performance in force exertion, velocity, stiffness, energy efficiency, and precision.

Future improvement of our hybrid system could include: (1) achieving untethered actuation. (2) achieving actively control of the spring length during the motion of the BHSBA, possibly driven by DC motor or using shape memory spring. This active control could enable programmability in force, velocity, energy barrier, and stiffness of BHSBA, therefore allowing the crawler or swimmer to change speed and achieve new locomotion modes such as jumping or escaping. (3) optimizing the proposed clawer for faster locomotion. This could be achieved through optimizing the structure of BHSBA or replacing the rigid legs with energy-stored-legs. (4) constructing a modular hybrid robot (with BHSBA as a single module) that enables multiple-degree-of-freedom (for example, by positioning modules in orthogonal directions), multi-instability, and diverse utilities. (5) providing lock structure and spring tuning-mechanism for hybrid doming actuator to enable tunability in stiffness and bistability.

MATERIALS AND METHODS

Motion characterization

The motions of studied bending actuators (Fig. 2D) were captured by a Ximea USB3 (Serial number: MQ022CG-CM) high-speed camera with a 60 Hz external synchronization signal. The recording time was ten seconds generating 600 frames. The tracking method was based on simple linear iterative clustering method to generate some super-pixels followed by a 2D Kalman filter to predict the positions of actuators.

Fabrication of bending actuators

The pneumatic soft bending actuators without encapsulation were fabricated following the conventional molding-demolding manufacturing technique for fluid-driven soft actuators reported by Ref. (10). Encapsulated pneumatic bending actuators were fabricated following Ref. (39). The braided structure (denoted by red color in Fig. 3A) was prepared by compressing the polyester sleeve (McMaster-Carr, 9284K4) through a steel rod and then curing in the oven at 60° for 20 min. All rigid skeletons, mostly made of PLA, were 3D printed by Ultimaker 2+ and were bonded with the soft actuators by both Ecoflex 00-50 (Smooth-on Inc) and Insta-Cure glue (Bob Smith).

Fabrication of doming actuators

The detailed steps on the fabrication of entirely soft dome-bending actuators can be found in our previous work (30, 55). The fabrication of hybrid soft doming adhesion actuator (HSDAA) requires the rigid spine and the doming actuator (diameter = 100 mm) to be separately prepared as the first step. Then both of them are placed in a cylindrical mold (diameter = 120 mm) with the doming actuator on the top of the rigid skeleton. The following step is pouring uncured ecoflex into the mold until both the actuator and spine are totally submerged. After being degassed, the mold is positioned in oven at 45° for 4 hours and then the sample can be directly cast from the mold. For the shaft of the sliding beam (Fig. 6B), we used a polished stainless steel rod. The fabrication of bistable hybrid soft doming actuator (BHSDA) follows similar process as HSDAA. The only difference is that when positioning actuators and spine in the cylindrical mold, the spine is laminated between two doming actuators).

References

1. A. T. Baisch, O. Ozcan, B. Goldberg, D. Ithier, R. J. Wood, High speed locomotion for a quadrupedal microrobot. *Int. J. Robotics Res.* **33**, 1063-1082 (2014).
2. R. M. Alexander, Why Mammals Gallop1. *Am. Zool.* **28**, 237-245 (1988).
3. N. C. C. Sharp, Timed running speed of a cheetah (*Acinonyx jubatus*). *J. Zool.* **241**, 493-494 (1997).
4. R. M. Alexander, N. J. Dimery, R. F. Ker, Elastic structures in the back and their rôle in galloping in some mammals. *J. Zool.* **207**, 467-482 (1985).
5. B. M. Boszczyk, A. A. Boszczyk, R. Putz, Comparative and functional anatomy of the mammalian lumbar spine. *Anat. Rec.* **264**, 157-168 (2001).
6. N. Schilling, R. Hackert, Sagittal spine movements of small therian mammals during asymmetrical gaits. *J. Exp. Biol.* **209**, 3925-3939 (2006).
7. M. Hildebrand, Motions of the Running Cheetah and Horse. *J. Mammal.* **40**, 481-495 (1959).
8. Q. Zhao, B. Ellenberger, H. Sumioka, T. Sandy, R. Pfeifer, in *2013 IEEE International Conference on Robotics and Biomimetics (ROBIO)*. (2013), pp. 1807-1812.
9. J. Duperret, D. E. Koditschek, in *2017 IEEE International Conference on Robotics and Automation (ICRA)*. (2017), pp. 1058-1064.
10. R. F. Shepherd, F. Ilievski, W. Choi, S. A. Morin, A. A. Stokes, A. D. Mazzeo, X. Chen, M. Wang, G. M. Whitesides, Multigait soft robot. *Proc. Natl. Acad. Sci.* **108**, 20400-20403 (2011).
11. A. M. Nasab, A. Sabzehzar, M. Tatari, C. Majidi, W. Shan, A Soft Gripper with Rigidity Tunable Elastomer Strips as Ligaments. *Soft Robot.* **4**, 411-420 (2017).
12. K. C. Galloway, K. P. Becker, B. Phillips, J. Kirby, S. Licht, D. Tchernov, R. J. Wood, D. F. Gruber, Soft robotic grippers for biological sampling on deep reefs. *Soft Robot.* **3**, 23-33 (2016).
13. Y. Li, Y. Chen, T. Ren, Y. Li, S. H. Choi, Precharged Pneumatic Soft Actuators and Their Applications to Untethered Soft Robots. *Soft Robot.* **0**, null (2018).
14. R. Deimel, O. Brock, A novel type of compliant and underactuated robotic hand for dexterous grasping. *Int. J. Robotics Res.* **35**, 161-185 (2016).
15. P. Polygerinos, Z. Wang, K. C. Galloway, R. J. Wood, C. J. Walsh, Soft robotic glove for combined assistance and at-home rehabilitation. *Rob. Auton. Syst.* **73**, 135-143 (2015).
16. E. Brown, N. Rodenberg, J. Amend, A. Mozeika, E. Steltz, M. R. Zakin, H. Lipson, H. M. Jaeger, Universal robotic gripper based on the jamming of granular material. *Proc. Natl. Acad. Sci.* **107**, 18809-18814 (2010).

17. E. W. Hawkes, L. H. Blumenschein, J. D. Greer, A. M. Okamura, A soft robot that navigates its environment through growth. *Sci. Robot.* **2**, eaan3028 (2017).
18. A. D. Marchese, R. Tedrake, D. Rus, Dynamics and trajectory optimization for a soft spatial fluidic elastomer manipulator. *Int. J. Robotics Res.* **35**, 1000-1019 (2016).
19. R. V. Martinez, J. L. Branch, C. R. Fish, L. Jin, R. F. Shepherd, R. M. D. Nunes, Z. Suo, G. M. Whitesides, Robotic Tentacles with Three-Dimensional Mobility Based on Flexible Elastomers. *Adv. Mater.* **25**, 205-212 (2013).
20. M. A. Robertson, J. Paik, New soft robots really suck: Vacuum-powered systems empower diverse capabilities. *Sci. Robot.* **2**, eaan6357 (2017).
21. M. Cianchetti, T. Ranzani, G. Gerboni, T. Nanayakkara, K. Althoefer, P. Dasgupta, A. Menciassi, Soft Robotics Technologies to Address Shortcomings in Today's Minimally Invasive Surgery: The STIFF-FLOP Approach. *Soft Robot.* **1**, 122-131 (2014).
22. D. Drotman, S. Jadhav, M. Karimi, M. T. Tolley, in *Robotics and Automation (ICRA), 2017 IEEE International Conference on.* (IEEE, 2017), pp. 5532-5538.
23. P. Glick, S. Suresh, D. Ruffatto III, M. Cutkosky, M. T. Tolley, A. Parness, A soft robotic gripper with gecko-inspired adhesive. *IEEE Robot. Autom. Lett.* **3**, 4201-4208, (2018).
24. U. Culha, J. Hughes, A. Rosendo, F. Giardina, F. Iida, in *Soft Robotics: Trends, Applications and Challenges.* (Springer, 2017), pp. 87-94.
25. A. A. Stokes, R. F. Shepherd, S. A. Morin, F. Ilievski, G. M. Whitesides, A Hybrid Combining Hard and Soft Robots. *Soft Robot.* **1**, 70-74 (2014).
26. T. Chen, O. R. Bilal, K. Shea, C. Daraio, Harnessing bistability for directional propulsion of soft, untethered robots. *Proc. Natl. Acad. Sci.* **115**, 5698-5702 (2018).
27. P. Rothemund, A. Ainla, L. Belding, D. J. Preston, S. Kurihara, Z. Suo, G. M. Whitesides, A soft, bistable valve for autonomous control of soft actuators. *Sci. Robot.* **3**, eaar7986 (2018).
28. J. T. B. Overvelde, T. Kloek, J. J. A. D'haen, K. Bertoldi, Amplifying the response of soft actuators by harnessing snap-through instabilities. *Proc. Natl. Acad. Sci.* **112**, 10863-10868 (2015).
29. B. Shin, J. Ha, M. Lee, K. Park, G. H. Park, T. H. Choi, K.-J. Cho, H.-Y. Kim, Hygrobot: A self-locomotive ratcheted actuator powered by environmental humidity. *Sci. Robot.* **3**, eaar2629 (2018).
30. Y. Tang, Q. Zhang, G. Lin, J. Yin, Switchable Adhesion Actuator for Amphibious Climbing Soft Robot. *Soft Robot.* <http://doi.org/10.1089/soro.2017.0133> (2018).
31. S. Seok, C. D. Onal, K.-J. Cho, R. J. Wood, D. Rus, S. Kim, Meshworm: a peristaltic soft robot with antagonistic nickel titanium coil actuators. *IEEE ASME Trans. Mechatron.* **18**, 1485-1497 (2013).
32. T. Umedachi, V. Vikas, B. Trimmer, Softworms: the design and control of non-pneumatic, 3D-printed, deformable robots. *Bioinspir. Biomim.* **11**, 025001 (2016).
33. C. D. Onal, D. Rus, Autonomous undulatory serpentine locomotion utilizing body dynamics of a fluidic soft robot. *Bioinspir. Biomim.* **8**, 026003 (2013).
34. L. Shi, S. Guo, K. Asaka, S. Mao, in *Nano/Molecular Medicine and Engineering (NANOMED), 2010 IEEE 4th International Conference on.* (IEEE, 2010), pp. 1-6.
35. C. T. Nguyen, H. Phung, H. Jung, U. Kim, T. D. Nguyen, J. Park, H. Moon, J. C. Koo, H. R. Choi, in *Robotics and Automation (ICRA), 2015 IEEE International Conference on.* (IEEE, 2015), pp. 4484-4489.
36. J. Cao, L. Qin, J. Liu, Q. Ren, C. C. Foo, H. Wang, H. P. Lee, J. Zhu, Untethered soft robot capable of stable locomotion using soft electrostatic actuators. *Extreme Mech. Lett.* **21**, 9-16 (2018).
37. W.-B. Li, W.-M. Zhang, H.-X. Zou, Z. Peng, G. Meng, A Fast Rolling Soft Robot Driven by Dielectric Elastomer. *IEEE ASME Trans. Mechatron.* **23**, 1630 - 1640 (2018).

38. M. Duduta, D. R. Clarke, R. J. Wood, in *Robotics and Automation (ICRA), 2017 IEEE International Conference on*. (IEEE, 2017), pp. 4346-4351.
39. M. Cianchetti, T. Ranzani, G. Gerboni, I. De Falco, C. Laschi, A. Menciassi, in *Intelligent Robots and Systems (IROS), 2013 IEEE/RSJ International Conference on*. (IEEE, 2013), pp. 3576-3581.
40. F. G. Serchi, A. Arienti, C. Laschi, Biomimetic vortex propulsion: toward the new paradigm of soft unmanned underwater vehicles. *IEEE ASME Trans. Mechatron.* **18**, 484-493 (2013).
41. S.-H. Song, M.-S. Kim, H. Rodrigue, J.-Y. Lee, J.-E. Shim, M.-C. Kim, W.-S. Chu, S.-H. Ahn, Turtle mimetic soft robot with two swimming gaits. *Bioinspir. Biomim.* **11**, 036010 (2016).
42. T. Li, G. Li, Y. Liang, T. Cheng, J. Dai, X. Yang, B. Liu, Z. Zeng, Z. Huang, Y. Luo, Fast-moving soft electronic fish. *Sci. Adv.* **3**, e1602045 (2017).
43. M. D. Bartlett, N. Kazem, M. J. Powell-Palm, X. Huang, W. Sun, J. A. Malen, C. Majidi, High thermal conductivity in soft elastomers with elongated liquid metal inclusions. *Proc. Natl. Acad. Sci.* **114**, 2143-2148 (2017).
44. J. Najem, S. A. Sarles, B. Akle, D. J. Leo, Biomimetic jellyfish-inspired underwater vehicle actuated by ionic polymer metal composite actuators. *Smart Mater. Struct.* **21**, 094026 (2012).
45. H. Jin, E. Dong, G. Alici, S. Mao, X. Min, C. Liu, K. Low, J. Yang, A starfish robot based on soft and smart modular structure (SMS) actuated by SMA wires. *Bioinspir. Biomim.* **11**, 056012 (2016).
46. R. K. Katzschmann, J. DelPreto, R. MacCurdy, D. Rus, Exploration of underwater life with an acoustically controlled soft robotic fish. *Sci. Robot.* **3**, eaar3449 (2018).
47. Y. Wei, Y. Chen, T. Ren, Q. Chen, C. Yan, Y. Yang, Y. Li, A Novel, Variable Stiffness Robotic Gripper Based on Integrated Soft Actuating and Particle Jamming. *Soft Robot.* **3**, 134-143 (2016).
48. Y. Yang, Y. Chen, in *Biomedical Robotics and Biomechatronics (BioRob), 2016 6th IEEE International Conference on*. (IEEE, 2016), pp. 195-200.
49. J. Shintake, B. Schubert, S. Rosset, H. Shea, D. Floreano, in *Intelligent Robots and Systems (IROS), 2015 IEEE/RSJ International Conference on*. (IEEE, 2015), pp. 1097-1102.
50. A. Balasubramanian, M. Standish, C. J. Bettinger, Microfluidic thermally activated materials for rapid control of macroscopic compliance. *Adv. Funct. Mater.* **24**, 4860-4866 (2014).
51. M. Manti, V. Cacucciolo, M. Cianchetti, Stiffening in soft robotics: a review of the state of the art. *IEEE Robot. Autom. Mag.* **23**, 93-106 (2016).
52. M. Manti, T. Hassan, G. Passetti, N. D'Elia, C. Laschi, M. Cianchetti, A Bioinspired Soft Robotic Gripper for Adaptable and Effective Grasping. *Soft Robot.* **2**, 107-116 (2015).
53. S. Mintchev, J. Shintake, D. Floreano, Bioinspired dual-stiffness origami. *Science Robotics* **3**, eaau0275 (2018).
54. J. A. Faber, A. F. Arrieta, A. R. Studart, Bioinspired spring origami. *Science* **359**, 1386-1391 (2018).
55. Y. Tang, J. Yin, Design of Multifunctional Soft Doming Actuator for Soft Machines. *Adv. Mater. Technol.* **3**, 1800069 (2018).
56. M. T. Tolley, R. F. Shepherd, M. Karpelson, N. W. Bartlett, K. C. Galloway, M. Wehner, R. Nunes, G. M. Whitesides, R. J. Wood, in *Intelligent Robots and Systems (IROS 2014), 2014 IEEE/RSJ International Conference on*. (IEEE, 2014), pp. 561-566.
57. A. Pandey, D. E. Moulton, D. Vella, D. P. Holmes, Dynamics of snapping beams and jumping poppers. *Europhys. Lett.* **105**, 24001 (2014).

58. L. Freund, J. Floro, E. Chason, Extensions of the Stoney formula for substrate curvature to configurations with thin substrates or large deformations. *Appl. Phys. Lett.* **74**, 1987-1989 (1999).
59. S. Kim, M. Spenko, S. Trujillo, B. Heyneman, D. Santos, M. R. Cutkosky, Smooth vertical surface climbing with directional adhesion. *IEEE Trans. Robot.* **24**, 65-74 (2008).
60. Y. Wang, X. Yang, Y. Chen, D. K. Wainwright, C. P. Kenaley, Z. Gong, Z. Liu, H. Liu, J. Guan, T. Wang, A biorobotic adhesive disc for underwater hitchhiking inspired by the remora suckerfish. *Sci. Robot.* **2**, eaan8072 (2017).
61. S. Russo, T. Ranzani, C. J. Walsh, R. J. Wood, An Additive Millimeter-Scale Fabrication Method for Soft Biocompatible Actuators and Sensors. *Adv. Mater. Technol.* **2**, 1700135 (2017).
62. E. T. Roche, M. A. Horvath, I. Wamala, A. Alazmani, S.-E. Song, W. Whyte, Z. Machaidze, C. J. Payne, J. C. Weaver, G. Fishbein, Soft robotic sleeve supports heart function. *Sci. Transl. Med.* **9**, eaaf3925 (2017).
63. P. Polygerinos, K. C. Galloway, S. Sanan, M. Herman, C. J. Walsh, in *Rehabilitation Robotics (ICORR), 2015 IEEE International Conference on.* (IEEE, 2015), pp. 55-60.

Acknowledgements: The authors acknowledge the helpful discussion with Dr. Andrew Spence and his help in high-speed motion capturing set-up. The authors thank Ms. Shuaihua Jin for helping with the adult-body-weight holding testing of the high-strength hybrid doming adhesion actuator.

Author contributions: Y. T. and J. Y. developed the concept, designed the experiments, and analyzed the data. Y. T. fabricated and characterized the prototypes of bending and doming actuators and related locomotive robots, grippers, oscillator, and adhesion pads. Y. C. designed and conducted the testing of grippers with stiffness modulation through step motor driven tendons. O. H. M. conducted the data analysis on tracking the swing motion of bending actuators. J. Y. supervised the experiments. Y. T. and J. Y. wrote the manuscript. Y. C. and O. H. M. edited the manuscript.

Competing Interests: The authors declare that they have no competing interests.

SUPPLEMENTARY MATERIALS

Spined hybrid soft robot for high speed, high force, tunable bistability, and wide-range stiffness modulation

Yichao Tang¹, Yinding Chi¹, Omid H. Maghsoudi², Jie Yin^{1*}

¹Applied Mechanics of Materials Laboratory (AMML), Department of Mechanical Engineering, Temple University, 1947 North 12th Street, Philadelphia, PA 19122, USA.

²Department of Bioengineering, Temple University, 1947 North 12th Street, Philadelphia, PA 19122, USA.

* Corresponding author. Email: jjeyin@temple.edu

Text

Fig. S1. Schematics of patterned pneumatic channels in two-way soft bending actuator and structure of linked spine.

Fig. S2. Actuation timing control pattern for proposed hybrid actuators and robots.

Fig. S3. Experimental setup of bending stiffness measurements.

Fig. S4. Structure of rigid spines for bistable hybrid soft doming actuator (BHSDA).

Fig. S5. Bifurcation of bilayer doming structure.

Fig. S6. Prototype of hybrid soft doming adhesion actuator (HSDAA) and experimental set-up for holding a female adult through HSDAA.

Fig. S7. Schematic of the proposed skeleton for HSDAA.

Table. S1. Data of actuation pressure and time control pattern.

Movie S1. Slow motion of swinging of bistable hybrid soft bending actuator (BHSDA) captured by high-speed camera.

Movie S2. Realtime swing motion of bistable hybrid actuator, hybrid actuator, and soft actuator with the same swing angle of 60°.

Movie S3. Realtime locomotion of three bending actuator-based crawlers on a horizontal surface.

Movie S4. Slow motion ($\times 0.125$) of spined bistable hybrid soft crawler locomoting on a horizontal surface.

Movie S5. Realtime climbing of three bending actuator-based crawlers on a slightly tilted surface.

Movie S6. Realtime underwater locomotion of three bending actuator-based fish-like soft robots.

Movie S7. Demonstrations of strength-adjustable hybrid soft grippers in grasping a variety of objects ranging from fragile lightweight to high-load objects.

Movie S8. Demonstration of bistable soft doming oscillator.

Movie S9. Demonstration of hybrid soft doming adhesion actuator (HSDAA) as a high strength adhesive device to hold a female adult.

Text

Energy barrier and consumption in bistable hybrid soft bending actuator (BHSBA)

To enable the snap-through bistability and save the energy, the energy barrier E of BHSBA must satisfy

$$E = U_{Spring,II} - (U_{Spring,I} + U_{actuator,I}) < E_{input} < U_{actuator,I} \quad (S-1)$$

where E_{input} is the energy consumption of the system. This equation can be easily simplified as:

$$\frac{1}{2} k \Delta x^2 \cdot \sin^2\left(\frac{\theta_l}{2}\right) < 2U_{actuator,I} \quad (S-2)$$

where k is the stiffness of the spring and Δx presents the extension of the spring at state II. θ_l is the lock angle. The strain energy of the pneumatic soft bending actuators at rest states $U_{actuator,I}$ can be approximately obtained as through homogenization:

$$U_{actuator,I} \approx \int_V \frac{1}{2} E \left[\frac{2y \tan(\theta_l/2)}{L} \right]^2 dV + \int_V \frac{1}{2} E \left[1 - \frac{\theta_l}{2 \tan(\theta_l/2)} \right]^2 dV \quad (S-3)$$

where L is the length of the spine. E is the Young's modulus. The first and second term represents the bending and stretching energy in the soft bending actuators, respectively. It should be noted that the model is oversimplified through homogenization without considering its detailed pneumatic channels. It also assumes the idealized linear elastic materials behavior in the homogenized continuous layer despite the nonlinear deformation in the elastomer.

From Eq. (S-2), we can see that when the spring stiffness or extension is relatively small, the BHSBA cost less energy than its soft counterparts to achieve the same bending angle. When the spring stiffness or pre-extension is set to be too large, it will readily satisfy Eq. (S-2). However, in this case, BHSBA will require more energy input than its soft counterpart to achieve the same bending angle. Meanwhile, BHSBA with a high-stiffness spring yields a much higher force output than the soft actuator. Therefore, a trade-off in selecting spring should be considered for different conditions.

Curvature of BHSBA

With the help of the proposed rigid spine, BHSBA demonstrates a nominal uniform curvature, which is hard to be achieved by its counterpart soft bending actuator. Its curvature, κ , can be obtained as:

$$\kappa = \frac{2 \tan(\theta_l/2)}{L} \quad (\text{S-4})$$

Bending stiffness of BHSBA

The block force of BHSBA as a function of spring extension shown in Fig. 5C can be obtained as:

$$F_1 = k(\Delta x_1 + \Delta x) \sin\left(\frac{\theta_l}{2}\right) \frac{L_1}{L} \quad (\text{S-5})$$

Where Δx_l represents the pre-stretched length of the spring at rest state. L_l denotes the distance between the anchored points of the spring. In this equation, we ignore the effect of the bending actuators because the high-stiffness spring has much higher potential energy than the straining energy of the soft actuators at lock state (before lock state, this assumption is not valid). This assumption explains the slight disparity between the model and experimental results in predicting the block force. Similarly, the block force of BHSBA shown in Fig. 5B can be obtained as:

$$F_2 = \frac{k(\Delta x_1 + \Delta x) \sin(\theta_l/2)}{\cos(\theta_l)} \frac{L_1}{L} \quad (\text{S-6})$$

Figures

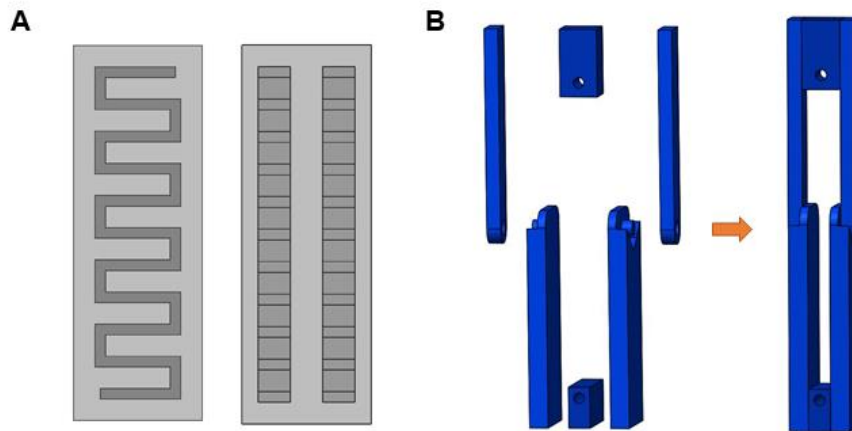


Fig. S1. Schematics of patterned pneumatic channels in two-way soft bending actuator and structure of linked spine. (A) Schematics of top view (left) and side view (right) of two-way pneumatic bending actuator that we use for bistable hybrid bending actuator (BHSBA). The darker color represents the patterned channel. (B) Exploded schematics of structure of the 3d-printed spine for BHSBA.

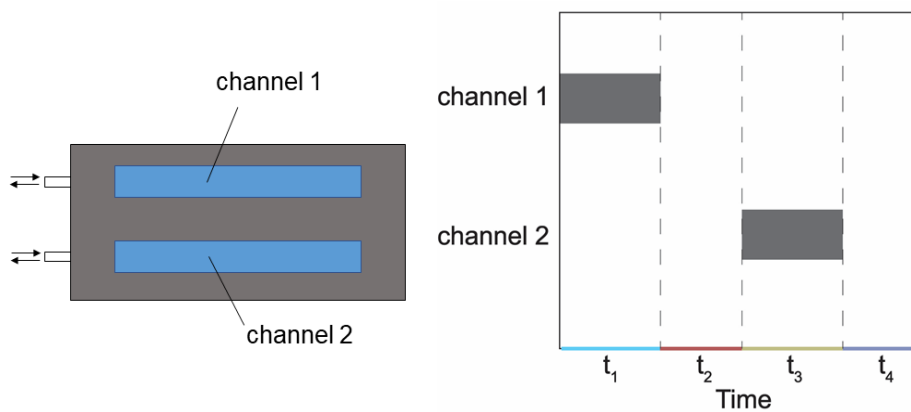


Fig. S2. Actuation timing control pattern for proposed hybrid actuators and robots. The grey lines in the right figure shows when a channel is pressurized. At all other times, channels are not actuated. The detailed data for controlling the proposed actuators and machines can be found in Table. S1.

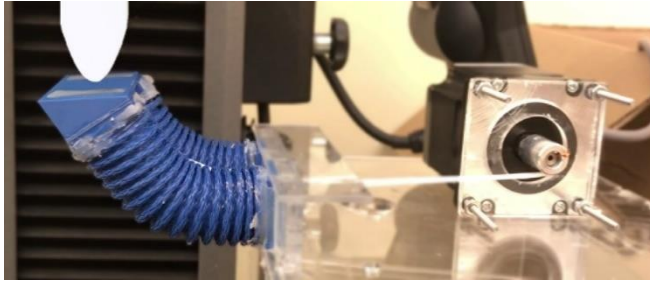


Fig. S3. Experimental setup of bending stiffness measurements. The force (blocked at 80°) is recorded by an Instron machine while the motor (AutomationDirect) is pulling the spring at a rate of 5 rpm.

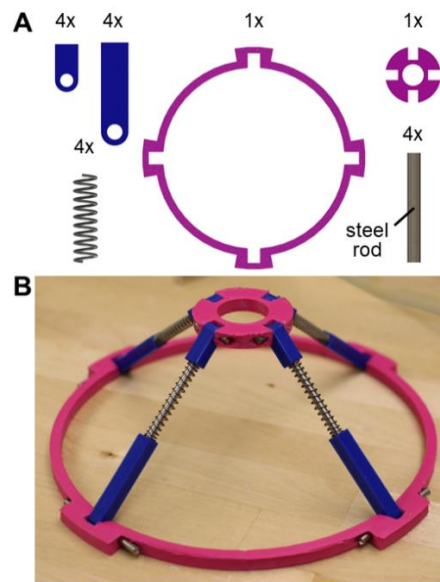


Fig. S4. Structure of rigid spines for bistable hybrid soft doming actuator (BHSDA). (A) the sub-components of the doming spine. (B) the proposed spine at rest states.

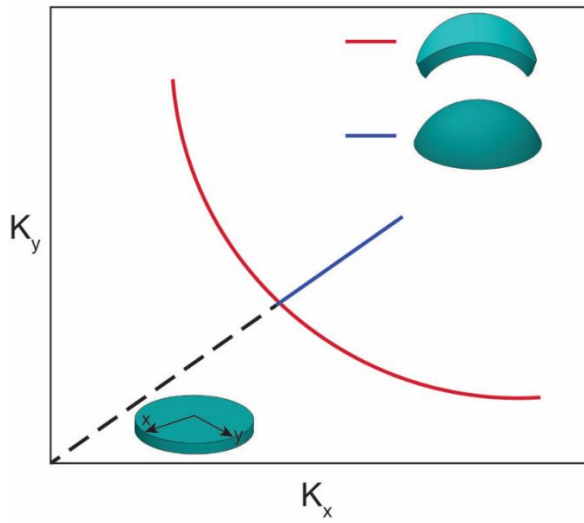


Fig. S5. Bifurcation of bilayer doming structure. With the increasing of the mismatching strain in the bilayer, the axisymmetric dome-shape configuration ($K_x = K_y$, the principle curvature along two orthogonal directions) will eventually transit into an asymmetric one ($K_x \neq K_y$, top inset). The detailed information can be found in Ref. (58). However, by integrating rigid spine into the doming actuator, this bifurcation can be eliminated because the spine possesses single degree of freedom, thus enabling only axisymmetric deformation.

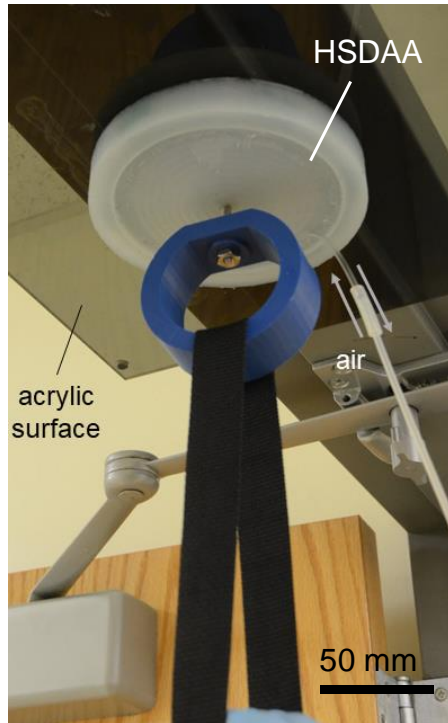


Fig. S6. Prototype of hybrid soft doming adhesion actuator (HSDAA) and experimental set-up for holding a female adult through HSDAA. The HSDAA is applied onto an acrylics surface (fixed on the doorframe) and pressured at 80 kPa.

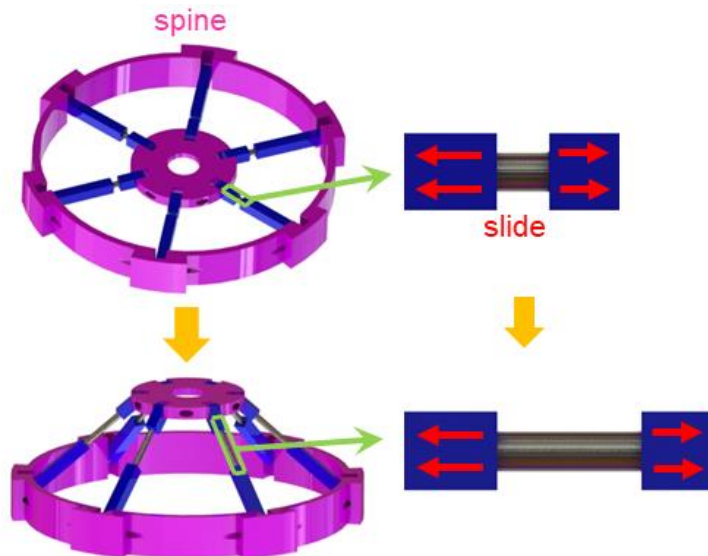


Fig. S7. Schematic of the proposed skeleton for HSDAA. The sliding of beams enables the pop-up or pop-down of the structure.

Table. S1. Data of actuation pressure and time control pattern

actuators / robots	P (kPa)	t ₁ (s)	t ₂ (s)	t ₃ (s)	t ₄ (s)
BHSBA (Fig. 2D)	30	0.09	0.07	0.09	0.07
crawler (Fig. 3)	30	0.09	0.07	0.09	0.07
swimmer (Fig. 4)	160	0.15	0.23	0.15	0.23
dome oscillator (Fig. 6)	100	0.3	0.25	0.3	0.25

The actuation timing control pattern is shown in Fig. S2.

Movie captions

Movie S1. Slow motion of swinging of bistable hybrid soft bending actuator (BHSBA)

captured by high-speed camera. The actuator is pressurized at 30 kPa and 3.2 Hz average frequency.

Movie S2. Realtime swing motion of bistable hybrid actuator, hybrid actuator, and soft

actuator with the same swing angle of 60°. When pressurized at 30 kPa, it takes bistable hybrid actuator 0.13s to transit from state I to state III and achieve 60° bending angle (average frequency = 3.85 Hz). It takes soft actuator 0.16 s (need to be pressurized at 38 kPa) to achieve the same bending angle. Hybrid actuator requires the highest pressure (80 kPa) to achieve the same deformation with the slowest speed (0.27 s).

Movie S3. Realtime locomotion of three bending actuator-based crawlers on a horizontal

surface. All actuators are pressured at 30 kPa with a 3.2 Hz average frequency. All crawlers are 7 cm long and 6 cm wide with a mass of 45g. The prototype built with BHSBA shows the fastest locomotion speed (2.49 BL/s or 174.4 mm/s). Crawler based on springless HSBA shows the slowest velocity (0.53 BL/s or 37.1 mm/s). Crawler based on SBA without spines can achieve locomotion at 1.19 BL/s, or 83.3 mm/s.

Movie S4. Slow motion ($\times 0.125$) of spined bistable hybrid soft crawler locomoting on a horizontal surface. Due to the amplified force and velocity enabled by the bistable structure, we observe the lift-off of both foreleg and hind legs from the surface during the locomotion.

Movie S5. Realtime climbing of three bending actuator-based crawlers on a slightly tilted surface. All actuators are pressured at 30 kPa with a 3.2 Hz average frequency. Crawler built with BHSBA can locomote on a 17° tilted surface with a 0.56 BL/s locomotion velocity while crawler based on SBA and HSBA do not show capabilities to climb such surfaces.

Movie S6. Realtime underwater locomotion of three bending actuator-based fish-like soft robots. The prototype is ~ 150 mm long with a mass of 51 g. The composed bending actuator is 45 mm in length and 25 mm in diameter. We use a stiff plastic film (0.25 mm) for the fish fin. The prototype built with BHSBA can locomote at 0.78 BL/s, or 117 mm/s. Crawler based on springless HSBA shows the slowest velocity (0.27 BL/s or 40 mm/s). Crawler based on soft actuators SBA can achieve locomotion at 0.58 BL/s, or 87 mm/s.

Movie S7. Demonstrations of strength-adjustable hybrid soft grippers in grasping a variety of objects ranging from fragile lightweight to high-load objects. Pneumatic actuation is used for gripping lightweight and fragile objects and motor-driven actuation is used for grasping large and heavy objects through pulling the spring. We first show the proposed gripper can manipulate a few lightweight objects including a fresh egg, steel wrap, a glass bottle and a tape. All actuators are pressurized at 90 kPa. Then we demonstrate the proposed gripper can hold heavier objects with weights of 600 g, 3.6 kg, 9.2 kg and 11.4 kg. The corresponding stretched lengths of the spring ($k = 9.7$ N/mm) at lock state (85°) are ~ 0.1 mm, ~ 3 mm, ~ 2 mm and ~ 3 mm. For the demonstration of grasping 9.2 kg and 11.4 kg payloads, an acrylics plate is fixed above the payload. Gripping these payloads is achieved through squeezing the acrylics plate first and then lifting the payloads.

Movies S8. Demonstration of bistable soft doming oscillator. The structure of the proposed oscillator is shown in Fig. 6A. The oscillation is achieved through repeatedly actuating the top and bottom channels in sequence, with 100 kPa pressure at an average frequency of 0.91 Hz.

Movie S9. Demonstration of hybrid soft doming adhesion actuator (HSDAA) as a high strength adhesive device to hold a female adult. We demonstrate the capability of proposed HSDAA to hold a female adult (52 kg). The HSDAA is applied onto an acrylic surface anchored to steel door frame and pressured at 80 kPa.